Investigating the remote-forcing hypothesis for upwelling in the Gulf of Guinea

Patrick Dwomfuor[1], Joseph K. Ansong[1*], Brian K. Arbic[2], Dimitris Menemenlis[3]

[1]Department of Mathematics, University of Ghana, Legon, Ghana.

[2]Department of Earth and Environmental Sciences, University of Michigan, Ann Arbor, Michigan, USA.

[3]Jet Propulsion Laboratory, California Institute of Technology, Pasadena, USA.

Corresponding author: Joseph K. Ansong, jkansong@ug.edu.gh

Abstract

Upwelling events in the Gulf of Guinea (GoG) impact climate and fisheries along the West African coastline. It has long been argued that the classical theory of coastal upwelling due to winds and Ekman transport is not the primary cause of the GoG upwelling. Rather, upwelling in the region has been hypothesized to be largely associated with Kelvin waves propagating eastward from the Brazilian coast along the equator. In this paper we test this hypothesis, using satellite observational data and output from the state-of-the-art Estimating the Circulation and Climate of the Ocean (ECCO) model. Kelvin waves are extracted from the satellite data and compared with those from the model. The phase speed of the Kelvin waves from satellite observations and model data is about 1.8 m/s, consistent with previous studies using only satellite observations. The correlations between the Kelvin waves (their displacements) from satellite observations and ECCO appear to increase in recent years, indicating model improvement. We also find high lagged correlation between the wind stress in the Brazilian region versus SST anomalies in the GoG region, from both satellite observations and model output, with a lag of about one month, thereby implicating the remote-forcing hypothesis for the GoG upwelling.

1 Plain Language Summary

There are several unanswered scientific questions regarding upwelling in the Gulf of Guinea. The classical paradigm of coastal upwelling involves Ekman transport (transport in the upper ocean that is directly driven by wind), but evidence suggests that the upwelling in the Gulf of Guinea may be different from the classical case. This knowledge led to the hypothesis that upwelling in the Gulf of Guinea is likely caused by equatorial Kelvin waves generated around the Brazilian coast propagating towards the Gulf of Guinea, bringing cold water. However, earlier studies lacked enough observational and realistic model data to validate or evaluate the hypothesis of remote forcing. This study revisits and tests the hypothesis using relatively recent satellite observational data and output from state-of-the-art numerical models such as the Estimating the Circulation and Climate of the Ocean (ECCO) model. The correlation between remote winds off the Brazilian coast and upwelling in the Gulf of Guinea is high, with a one-month lag time consistent with the time for Kelvin waves to travel across the Atlantic. On the other hand, the correlation between local winds and upwelling in the Gulf of Guinea is low.

2 Introduction

Upwelling is the process whereby cold water and nutrients from the deep ocean are displaced to the surface along coasts or along the equator. Upwelling events experienced in the Gulf of Guinea impact the climate along the West African coastline. Along the Gulf of Guinea, a major upwelling period is usually experienced from June to September, characterised by the seasonally low Sea Surface Temperature (SST) of the ocean, while a minor upwelling period usually occurs in January and February. During upwelling events, there is an increase in biological activities. For instance, there is an increase in phytoplankton and zooplankton, at the bottom of the food chain, thus triggering an increase in activity farther up the food chain. The increase in fish catch in areas that experience coastal upwelling is an important driver of local economies. Secondly, the cold water from upwelling in the Gulf of Guinea impacts West African climate (e.g., *Kouadio et al.* [2013]).

An important lingering question is whether Gulf of Guinea upwelling is forced by local versus remote factors. Previous studies (e.g., *O'Brien* [1978]; *Adamec et al.* [1978]; *Picaut* [1983]; *Wiafe et al.* [2015]) suggest that upwelling in the Gulf of Guinea is not strongly linked to the local winds. Various mechanisms have been hypothesized for the Gulf of Guinea upwelling. The study by *Bakun* [1978] suggested that geostrophic adjustments of the Guinea Current and the Ekman transport underlie Gulf of Guinea coastal upwelling. However, *Philander* [1979] showed that the amplitude of upwelling induced by the Guinea Current is negligible compared to observations. *Moore et al.* [1978] used observations to suggest that seasonal upwelling events in the Gulf of Guinea are not connected with fluctuations of the local winds, but are instead caused by an increase in westward wind stress, which releases a strong upwelling signal that travels as an internal Kelvin wave eastward along the equatorial Atlantic. When this upwelling signal reaches the eastern boundary of Equatorial Guinea, it splits into waves traveling poleward in both hemispheres along the coast (e.g., *Roundy et al.,* [1982], *Tulich et al.* [2009]). A number of these coastally trapped Kelvin waves reflect as propagating westward Rossby waves and/or coastal Kelvin waves. *Moore et al.* [1978] suggested that a definite time lag must exist between an equatorially trapped upwelling signal and the coastal upwelling event, but there was not enough observational or realistic model data to test this idea at the time. *O'Brien* [1978] and *Adamec et al.* [1978] used a two-layer model of a linear and non-linear form of the Navier-Stokes equations respectively, with wind stress limited to the west-

ern part of the ocean basin, to simulate equatorial and coastal Kelvin waves. Their studies were the first to use simple models to test the potential of propagating internal Kelvin waves as a mechanism for Gulf of Guinea upwelling. However, their models lacked realistic topographic effects, coastal geometries, and background flows.

The remote forcing hypothesis has also been supported by *Picaut* [1983], *Katz et al.* [1977], and *Katz et al.* [1982], who suggested that the strengthening of westward wind stress along the equatorial Atlantic Ocean causes surface water to pile up against the western boundary around the Brazilian coast, thus initiating a zonal pressure gradient balanced by the wind stress. This process triggers Kelvin waves which propagate eastward at a speed of $c = \sqrt{g'H}$ where g' is the reduced gravity, and H is the height of the water column. *Servain et al.* [1982] analyzed historical observational data, employing lag correlation analysis, to show evidence of remote forcing of the Gulf of Guinea upwelling. However, it has been four decades since the study by *Servain et al.* [1982], and there have been a lot more observational data collected and major improvements in realistic (operational) numerical models. This paper revisits and test the hypothesis of *Moore et al.* [1978] using relatively recent satellite observational data and output from state-of-the-art numerical models like ECCO.

3 Two-layer theory

We briefly derive the solution to the two-layer theory for Kelvin wave propagation by *Adamec et al.* [1978]. They considered the following system of linear equations:

$$\begin{aligned} \frac{\partial u}{\partial t} - \beta y v + g' \eta_x &= \tau^x / \rho H \\ \frac{\partial v}{\partial t} + \beta y u + g' \eta_y &= \tau^y / \rho H \\ \frac{\partial \eta}{\partial t} + H\left(\frac{\partial u}{\partial x} + \frac{\partial v}{\partial y}\right) &= 0, \end{aligned}$$

where g' is the reduced gravity, u is the velocity in the zonal direction (x-direction), v is the velocity in the meridional direction (y-direction), η is the perturbation of the sea surface, H is the resting water column thickness on a flat bottom, β is an approximation which provides a linear variation of the Coriolis force along the equator, τ^x and τ^y are the wind stress in the zonal and meridional direction respectively. Assuming a wave

solution of form

$$\begin{pmatrix} u \\ v \\ \eta \end{pmatrix} = \mathrm{Re} \begin{pmatrix} U \\ 0 \\ A(y) \end{pmatrix} e^{\mathrm{i}(kx-\omega t)},$$

yields the displacement as

$$\begin{aligned} \eta(x,y,t) &= \left[\frac{a\omega}{\beta k} + \left(A_0 - \frac{a\omega}{\beta k}\right) e^{-\frac{\beta k}{2\omega} y^2}\right] e^{\mathrm{i}(kx-\omega t)} \\ &= \left[\frac{a\omega}{\beta k} + \left(A_0 - \frac{a\omega}{\beta k}\right) e^{-\frac{y^2}{2L_r^2}}\right] e^{\mathrm{i}(kx-\omega t)}, \end{aligned}$$

where $a = -\mathrm{i}\dfrac{\beta}{\omega g'}\tau^x/\rho H\, e^{-\mathrm{i}(kx-\omega t)}$, $L_r = \sqrt{c/\beta}$ is the equatorial deformation radius, $k = \pm\sqrt{\dfrac{\omega^2}{g'H}}$ is the wavenumber in the x direction, $c = \sqrt{g'H}$ is the phase speed, and the zonal velocity is given by $u = \dfrac{\mathrm{i}}{\omega}\left(-g'\dfrac{\partial \eta}{\partial x} + \tau^x/\rho H\right)$. A phase speed of $c \sim 1.0\,\mathrm{m/s}$ gives $L_r \sim 225\,\mathrm{km}$ and an e-folding length of $\sqrt{2}L_r = 318\,\mathrm{km}$.

For bounded solutions we require $k > 0$, implying that wave propagation is in the eastward direction. The solutions have maximum amplitude at the equator and decay exponentially with increasing latitude away from the equator. The Kelvin wave solution gives some insight into the wave characteristics (e.g., their spatial and time scales), and hence, how waves could be extracted and characterized from observational and model data. Kelvin waves have wavelengths of about 1,000 to 10,000 km and have a period of 25 to 95 days (e.g., *Polo et al.* [2008]). The filter employed to extract Kelvin waves uses both their spatial extent (wavelength) and time (period). Using methods provided in *Polito et al.* [2003], Kelvin waves are extracted from observational data and model output at about one-month, three-month, and six-month periods for analysis. We will also employ lag correlation analyses to understand the physical link between Kelvin waves and upwelling events in the Gulf of Guinea from these data sets.

4 Observational Data

We obtain altimeter gridded Sea Level Anomalies (SLA) data from Copernicus marine and Environment Monitoring Service (CMEMS; *CMEMS2019* [2019]). CMEMS are responsible for processing and distributing Duacs grided "allsat" Sea Level Anomaly (SLA), formally distributed by Aviso as seen in `https://doi.org/10.48670/moi00145`. The SLA was sampled daily from the 1/4 degree × 1/4 degree resolution data and spans from 01-01-1993 to 03-06-2020. Kelvin waves are extracted from the SLA via techniques presented in *Polito et al.* [2003] on the characterization of Rossby waves. The Kelvin wave

extraction was done for several spectral bands of the equatorial Atlantic basin ranging from 15° North to 15° South, and 50° West to 15° East. A finite impulse response (FIR) filter of *Polito et al.* [2003] was applied to the global SLA to extract the Kelvin waves for the Atlantic region.

Wind and SST products are obtained from ERA5, a fifth-generation ECMWF (European Centre for Medium-Range Weather Forecasts) reanalysis of the global climate and weather for the past 40 to 70 years, as stated in *Hersbach et al.* [2018]. The wind stress is obtained by multiplying the air density by the speed of the wind squared and by a drag coefficient of 0.002 (*Servain et al.* [1982]). 36-year time series from 1981 to 2016 of monthly means of wind and SST was used to construct a monthly climatology of wind stress and SST anomalies.

5 Model Output (ECCO)

Model output is obtained from the Estimating the Circulation and Climate of the Ocean (ECCO) model. *Zhang et al.* [2018] and *Forget et al.* [2015] provide detailed documentation on the model output. The model employs the adjoint to reconstruct ocean states that minimize misfits between the model and observational data from satellites such as the Topex/Poseidon altimeter as well as in-situ measurements. The ECCO model-observational fit is performed while obeying the dynamical constraints of the underlying model equations. Data fitting is done by altering a set of ocean model initial conditions, parameters, and atmospheric boundary conditions that obey the laws of physics and thermodynamics. The version of the ECCO product used here is ECCO LLC270 (1/3 degree), which was interpolated to a 1/4 degree latitude-longitude (lat-lon) grid. SST and SSH were obtained from the ECCO LLC270 output product. SLA from Aviso and SSH from ECCO are both 1/4 degree.

6 Methodology

Using satellite observations from Copernicus (formerly AVISO), we denote the Sea Surface Height (SSH) or Sea Level Anomaly (SLA) as η. The SLA data are composed of different signals whose characteristics differ in terms of their period, wavelength, frequency, amplitude, and phase speed. The SSH, η, as discussed by *Polito et al.* [2003] can be decomposed as:

$$\eta = \eta_R + \eta_T + \eta_K + \eta_E + \eta_N, \tag{1}$$

where η_R, η_T, η_K, η_E, and η_N, represent Rossby waves, tropical instability waves, Kelvin waves, mesoscale eddies, and non-propagating signals, respectively. We briefly discuss some of the signatures of Rossby waves. The characteristics of Kelvin waves from observations and the model will be discussed later. Rossby waves (η_R) are westward propagating waves with wavelengths of about 1,000 to 10,000 km long. Rossby waves have a period of months to years and cause a surface displacement of about 1 to 10 cm. Rossby waves are long, non-dispersive, and transport energy westwards, thus intensifying currents at the western boundary. Rossby wave energy and phase travel at about the same speed with a typical magnitude of 0.01 to 1.2 m/s. For instance, along latitude 0.125°N on the eastern equatorial Atlantic ocean, the Rossby waves with a period of 44 days, amplitude of 7 mm and wavelength of 2625 km have a phase speed of about 0.70 m/s. *Polito et al.* [2000], *Polito et al.* [2003], and *Oliveira et al.* [2013] used a filtering code to extract and characterize Rossby waves at a specified bandpass. Their filtering code generates a series of Hovmöller diagrams of SLA from observations (Topex/Poseidon) or model data. We modified the filtering code used by *Polito et al.* [2003] to characterize Kelvin waves in the eastern equatorial Atlantic ocean. Thus, from the global SLA data, we construct Hovmöller diagrams, and compute the phase speeds, amplitude and wavelengths of Kelvin waves at different periods.

7 Results

In this section, the variables η_{K1} (η_1), η_{K3} (η_3), and η_{K6} (η_6) are used to represent Kelvin waves extracted using three time periods: one month, three months, and six months, respectively.

7.1 Equatorial Kelvin Wave Signatures from Observations and ECCO

To demonstrate the methodology of extracting Kelvin waves from the data, we performed one month, three month, and six month bandpass filters on SSH signals from ECCO for the three wave periods. Figure 1 shows Hovmöller diagrams at latitude 0.125°N, and longitudes 45 °W to 12 °E for the year 1997. A rough estimation from the figures gives phase speeds of about 1.92 m/s, illustrated with white arrows on the left and middle panels. From left to right of Figure 1, we see that as the wave period increases the distance between wave crests (or troughs) also increases as expected. The phase speeds are consistent with those obtained by *Polo et al.* [2008] who analyzed oceanic Kelvin waves prop-

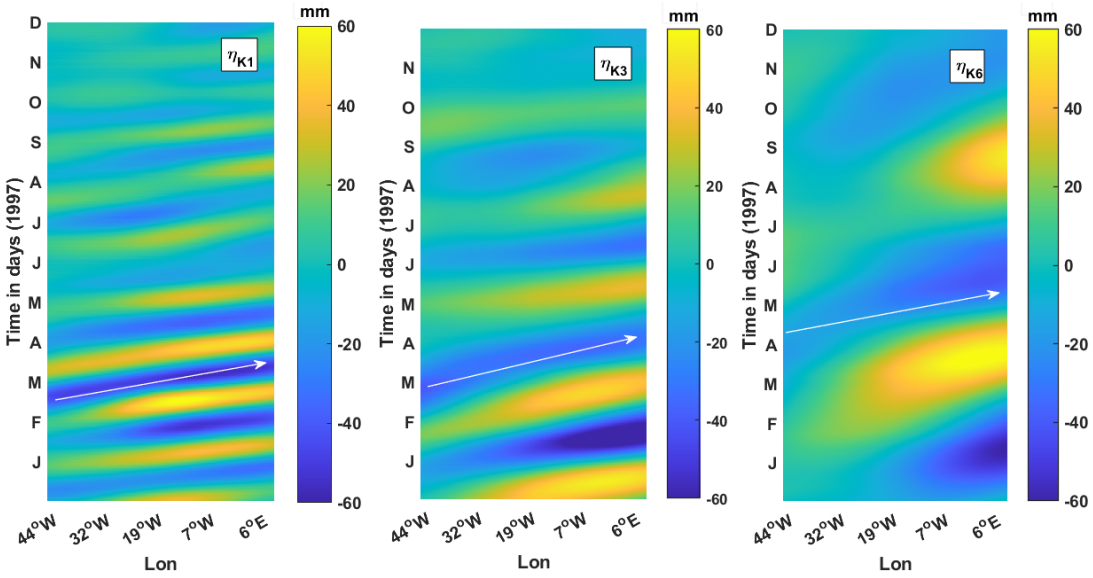

Figure 1: Kelvin waves from ECCO $\sim 1/3$ degree at latitude 0.125°N along the Atlantic ocean for the year 1997, where η_{K1}, η_{K3}, and η_{K6} correspond to Kelvin waves at one month, three month, and six month period respectively. The white arrows represent the slopes for the Kelvin waves suggesting a uniform phase speed of 1.92 m/s.

agating eastward in the tropical Atlantic region. The mean wave amplitudes are in the range 1.2–2.2 cm at the equator. The Kelvin waves at one-month period (Figure 1, left panel) appear to have larger amplitudes between January and May and relatively smaller amplitudes from June to December.

The spatial patterns of the equatorial Kelvin waves were also constructed to visualized their eastward propagation (as dictated by theory; Section 3) from the observational and model data, and to compare and contrast the two data sets. There are some years when Kelvin waves from observations and ECCO agree quite well. For example, in the year 2011, Kelvin waves from observations match well with ECCO (Figure 2). Figure 2a shows an almost symmetric height field of Kelvin waves around the equator with a latitudinal extent of about 300 km on either side of the equator, comparable to the e-folding length (see Section 3). The wave propagates eastward, and about two weeks later (Figure 2b) we find that the observational signal appears more symmetric about the equator than the signal in ECCO.

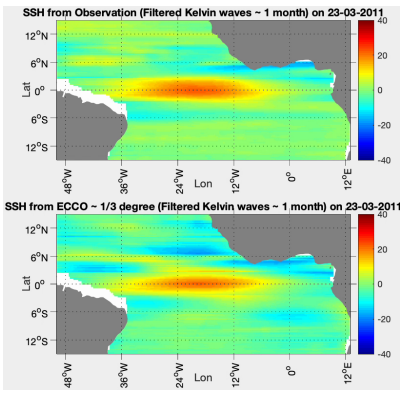

(a)

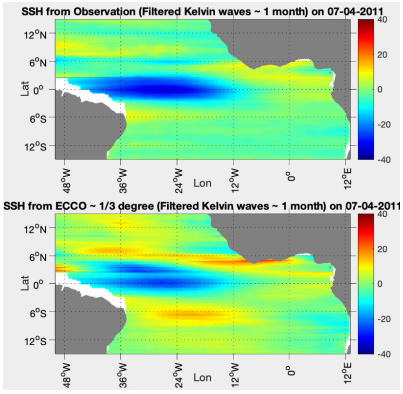

(b)

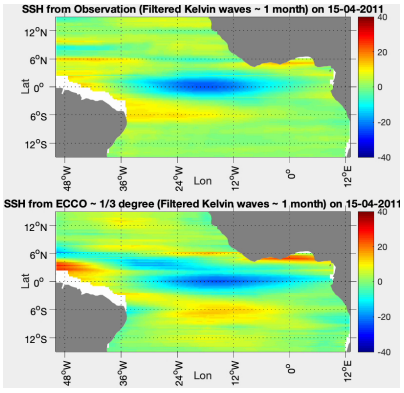

(c)

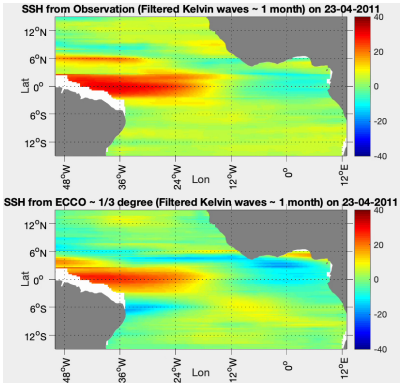

(d)

Figure 2: (a) Snapshots of Kelvin wave SSH from satellite observations (upper panels) and ECCO (lower panels) on March 25, 2011. Panels (b), (c) and (d) are the same as in (a) but at two week intervals. Waves are propagating from west to east in each panel.

The Hovmöller diagram in Figure 3 shows that the modeled Kelvin waves match very well to those from the satellite observations as seen in Figure 2. In both data sets, the waves have larger amplitudes between January and May and become less energetic from June to the end of the year. Lag correlation analysis will be used later to quantify the similarities and differences between the model and observations.

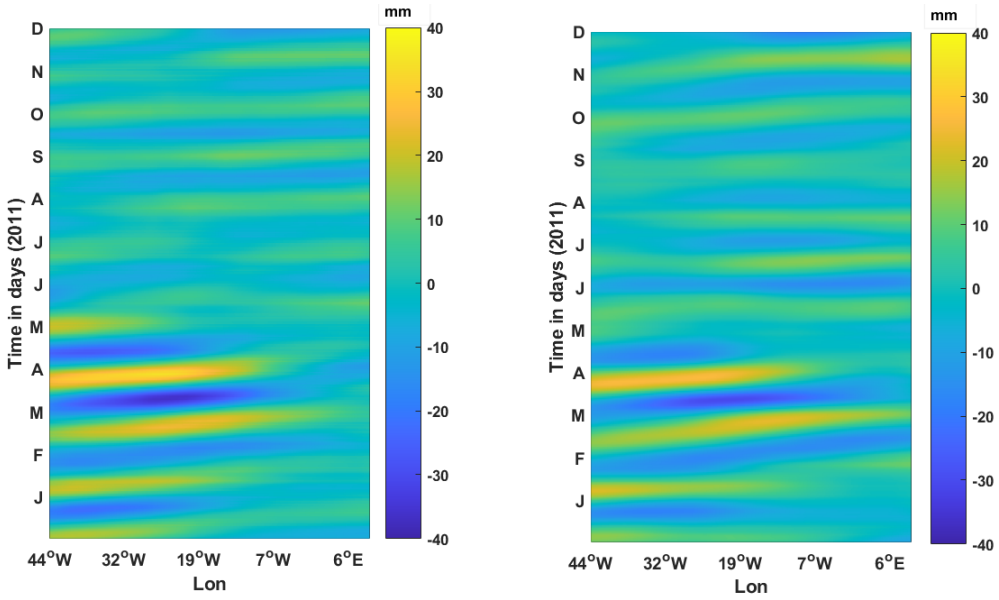

Figure 3: Kelvin waves (η_1) from satellite observation (left panel) and ECCO $\sim$1/3 (right panel) in the year 2011, constructed along latitude 0.125°N.

The spatial pattern and amplitude of Kelvin waves in ECCO do not always match well to those in the satellite observations (e.g. Figure 4) for some years. The wave signals are not as symmetric about the equator as in Figure 2 for both data sets. However, the amplitudes appear larger in ECCO (e.g., Figures 4b,c,d). This is more visible in Figure 5, constructed along latitude 0.125°N with wave period $T_{K1} = 44$ days and wavelength of 6726 km. The phase speed is about 1.8 m/s, which is consistent with the result of *Polo et al.* [2008]. Similarly, Kelvin waves extracted along the same latitude with period of $T_{K3} = 85$ days and wavelength of 12336 km have comparable phase speeds (1.8 m/s) in both data sets but the amplitudes in ECCO are larger than in the observations (Figure 6).

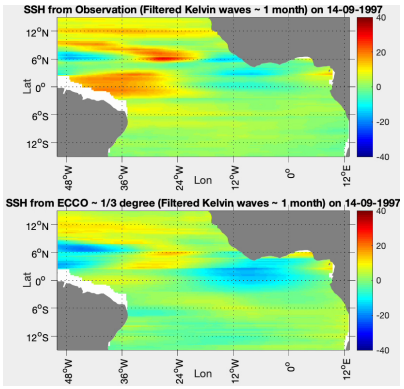

(a)

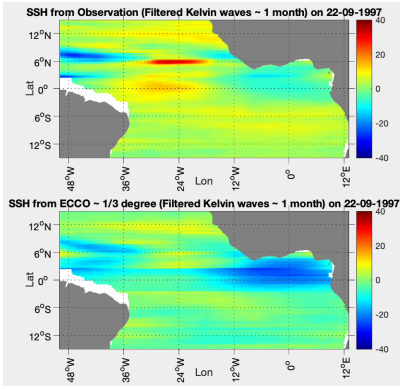

(b)

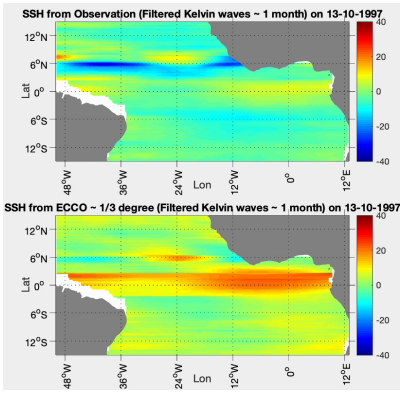

(c)

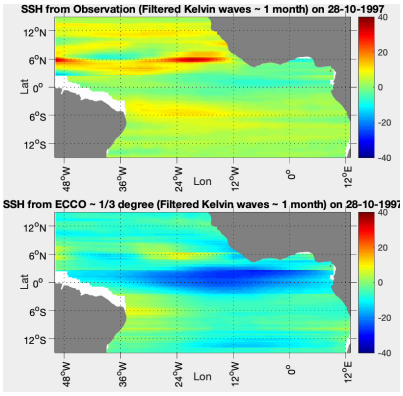

(d)

Figure 4: (a) Snapshots of Kelvin wave SSH from satellite observations (upper panels) and ECCO (lower panels) on September 14, 1997. Panels (b), (c) and (d) are the same as in (a) but at two week intervals. Waves are propagating from west to east in each panel.

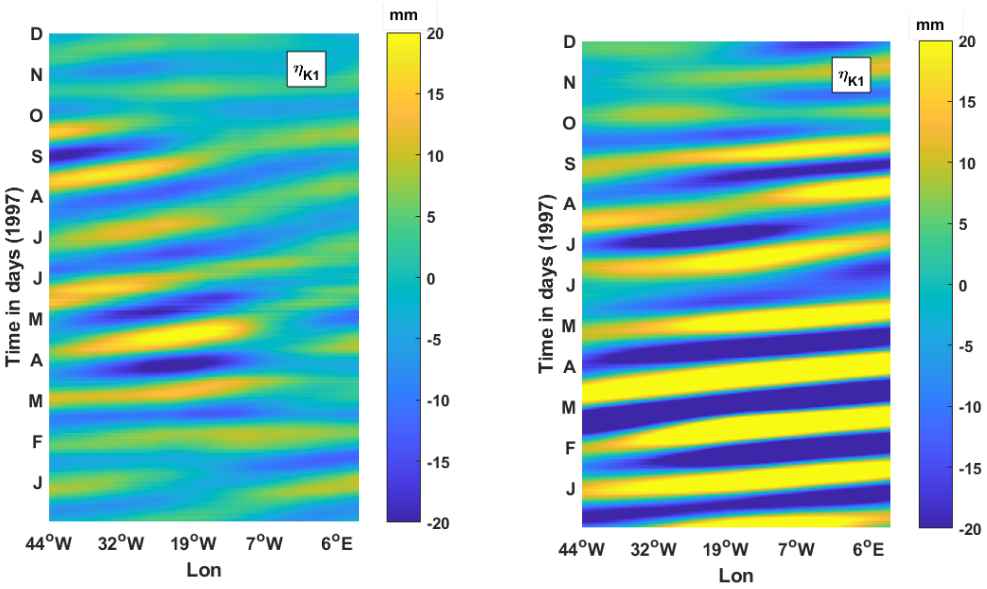

(a) (b)

Figure 5: Kelvin waves from satellite observations (left panel) and ECCO (right panel) for the year 1997 using 1.5 months bandpass filtering.

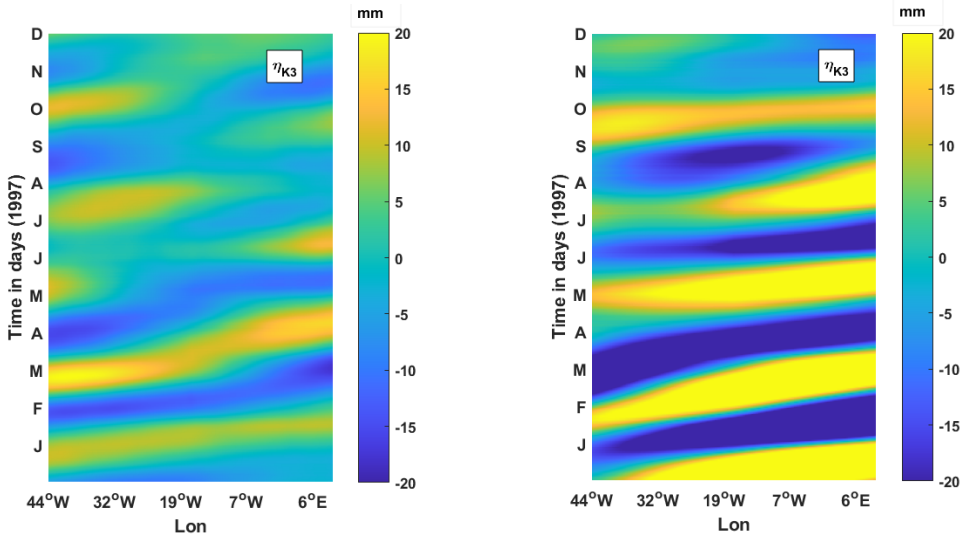

(a) (b)

Figure 6: Kelvin waves from satellite observations (left panel) and ECCO (right panel) for the year 1997 using 3 months bandpass filtering.

7.2 Relationship between Upwelling and Kelvin waves

In the previous section, we saw that the characteristics of Kelvin waves in ECCO and satellite observations are comparable to each other in some years, whereas they appear to be out of phase and to have differences in amplitudes in other years. In this section, lag correlation analysis is first used to quantify these differences and to determine whether ECCO has been improving over the years in capturing these equatorial Kelvin waves. We then perform lag correlation analysis to determine if there is high correlation between signals in the western equatorial Atlantic region and those from the Gulf of Guinea region in both observed and modeled data sets.

In Figures 2 and 3 (for 2011), we saw that the modeled and observed data matched quite well. A lag correlation analysis between the two data sets reveals a phase lag of 0 days with a correlation coefficient of 58.4% (Figure 7). Thus, in the year 2011, the two signals appear to be in phase and the difference in amplitudes yields the obtained correlation coefficient.

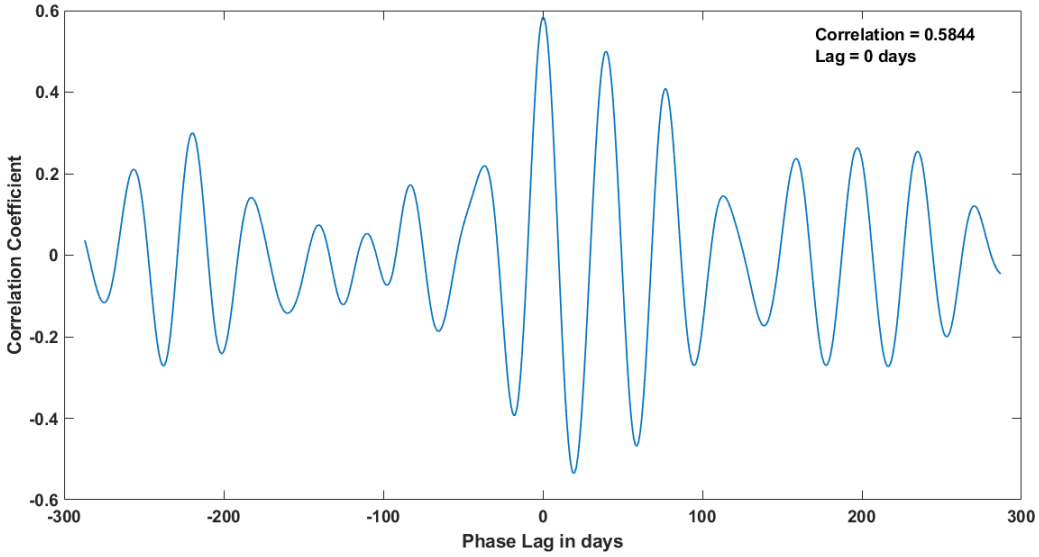

Figure 7: Lag correlation between Kelvin waves (η_1) from observations and Kelvin waves (η_1) from ECCO in the year 2011 from the Brazilian region.

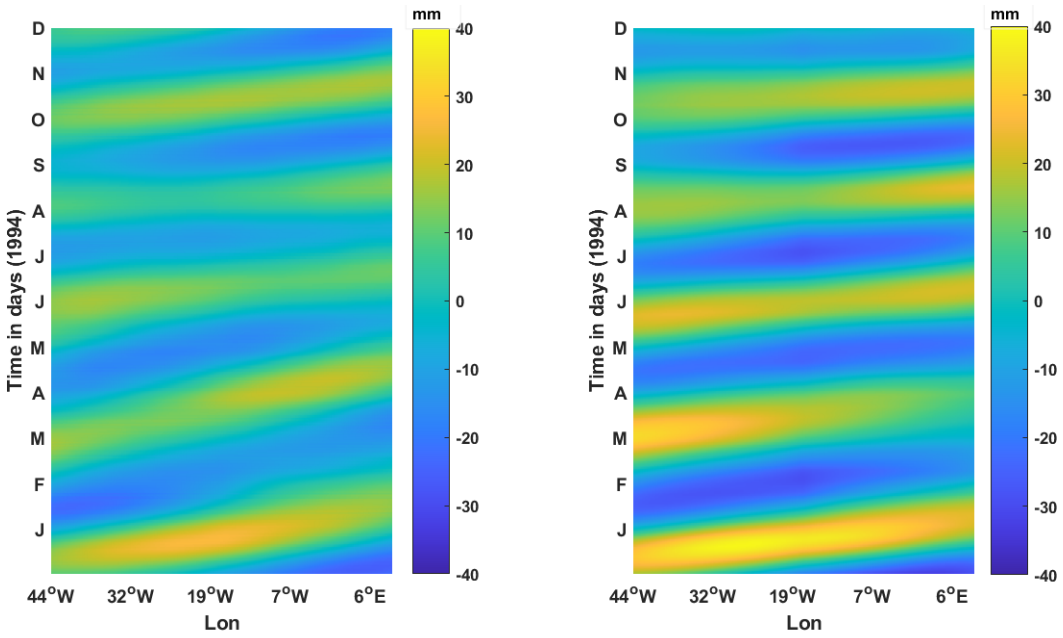

Figure 8: Hovmöller diagram of Kelvin waves (η_3) from satellite observations (left panel) and from ECCO∼1/3 (right panel) in the year 1994, and taken along latitude 0.125°N.

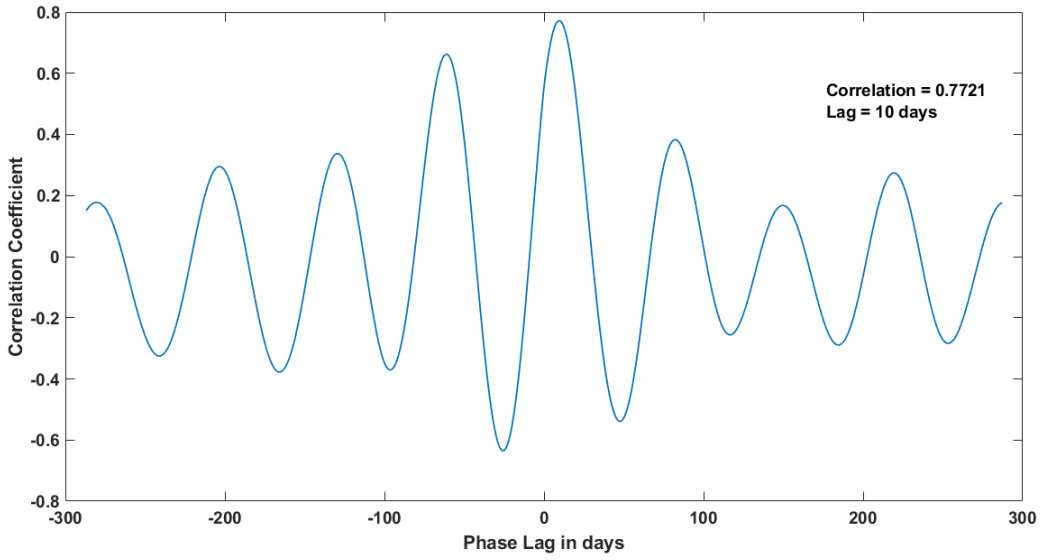

Figure 9: Lag correlation between Kelvin waves (η_3) from satellite observations compared with Kelvin waves (η_3) from ECCO in the year 1994 from the Guinea West of West Africa sub-region.

The Hovmöller diagram in Figure 8 shows Kelvin waves with about 3-month period from satellite observations and ECCO, with the amplitudes matching quite well. A lag correlation analysis indicates a high correlation coefficient of 77.2% but with a phase lag of 10 days, as shown in Figure 9.

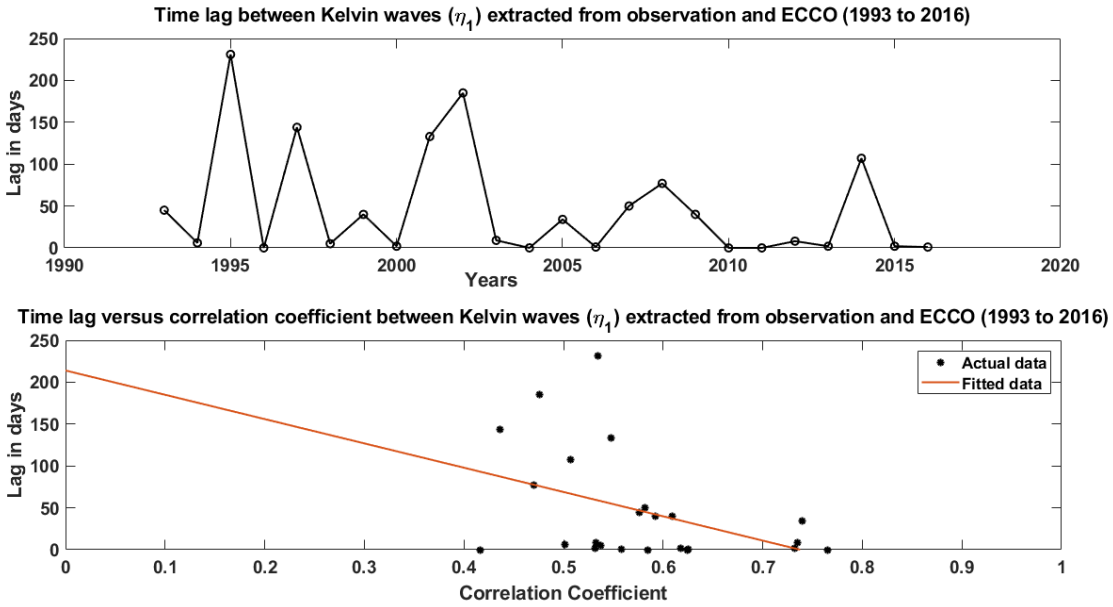

Figure 10: Lag correlation between Kelvin waves about one month (η_1) extracted from satellite observations and ECCO (1993 to 2016).

We next compute all the phase lags and correlation coefficients between model and satellite observations from 1994 to 2016 in the Brazilian region (BR) 5°N–5°S, 35°W–25°W to determine if there is some improvement in the modeling of equatorial Kelvin waves. Figure 10 (upper panel) shows that there appears to be a general decrease in phase lag between ECCO and satellite observations with time but the trend is not monotonic. This decreasing trend suggests an improvement in the model for simulating equatorial Kelvin waves. Similarly, it appears that signals with the highest correlation coefficients tend to have smaller phase lags (Figure 10, lower panel).

We now consider some selected areas of relevance in the Atlantic region as shown in Figure 11 to compute lag correlations between different fields to test the hypothesis of remote forcing by Kelvin waves. These areas include the Brazilian region (BR) 5°N–5°S, 35°W–25°W, Guinea North region (GN) 0°N–5°N, 10°W–10°E, Guinea West re-

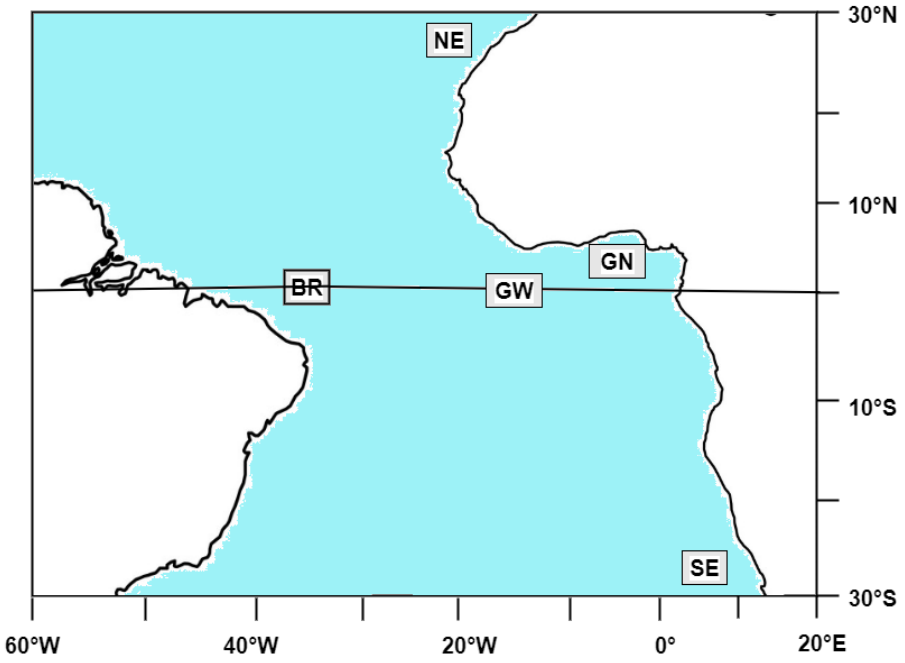

Figure 11: Selected areas of relevance in the Atlantic region as in *Servain et al.* [1982].

gion (GW) 5°N-5°S, 10°W-5°W, Northeastern region (NE), and Southeastern region (SE) as was done in *Servain et al.* [1982]. We let $\Delta\tau_x$ be the wind stress anomaly in the zonal direction, $\Delta\tau_y$ the wind stress in the meridional direction, and ΔSST the sea surface temperature anomaly. In Figure 12, we observe that the zonal wind stress anomaly in the Brazilian region (BR) correlates well with the SST anomaly in the Guinea West (GW) region (Figure 11). However, the correlation of the zonal wind stress and SST anomaly in the GW region is poor (Figure 13). This indicates that the local zonal winds have little or no effect on the low SST in the Gulf of Guinea. This suggests that upwelling in the Gulf of Guinea is not likely connected in any obvious way to the local winds, as indicated by *Bakun* [1978] and *Servain et al.* [1982].

Observational wind products and sea surface temperature (SST) data were obtained from ECMWF ERA5. The nonseasonal variations of SST and wind stress from zonal ($\Delta\tau_x$) and meridional ($\Delta\tau_y$) components were computed by subtracting the monthly mean values from the actual data. These monthly means were obtained by calculating monthly climatology from 1981 to 2016 to produce a 36-year time series. Similarly, for ECCO,

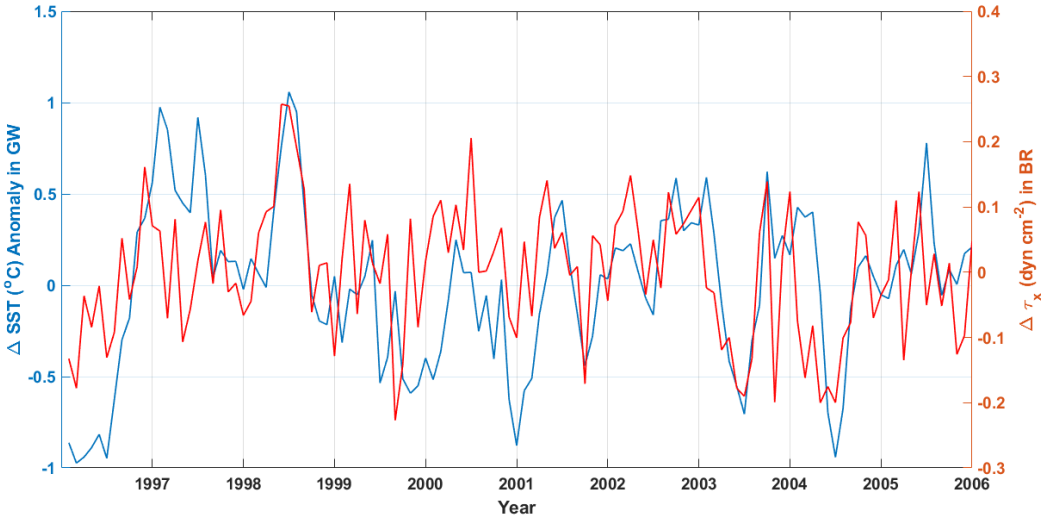

Figure 12: SST anomaly in Guinea West (GW) and zonal wind stress anomaly in Brazilian region (BR) from observations (1997 to 2006).

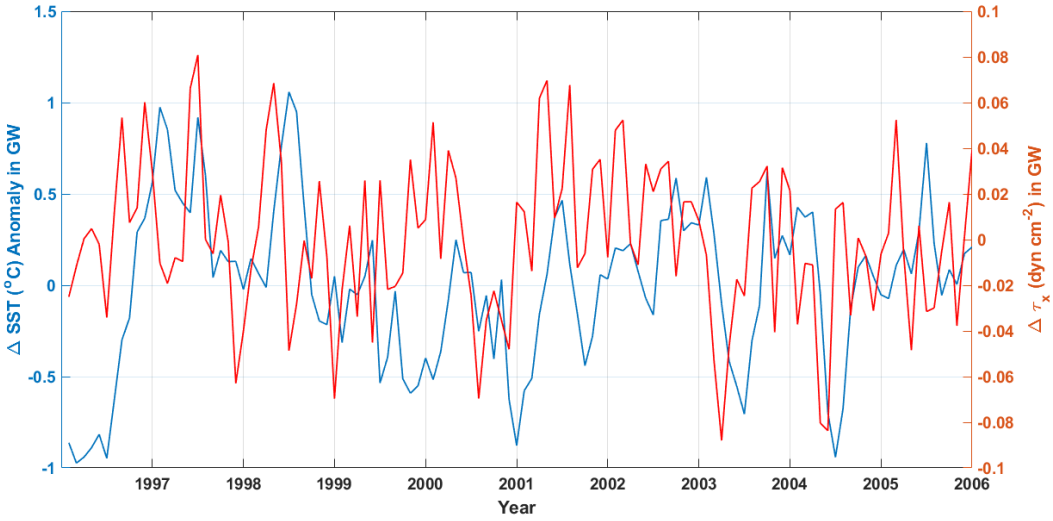

Figure 13: SST Anomaly in Guinea West region (GW) and zonal wind stress anomaly in Guinea West region (GW) from observations (1997 to 2006).

the SST monthly averages were obtained by calculating monthly climatologies from 1993 to 2016 to produce a 24-year time series.

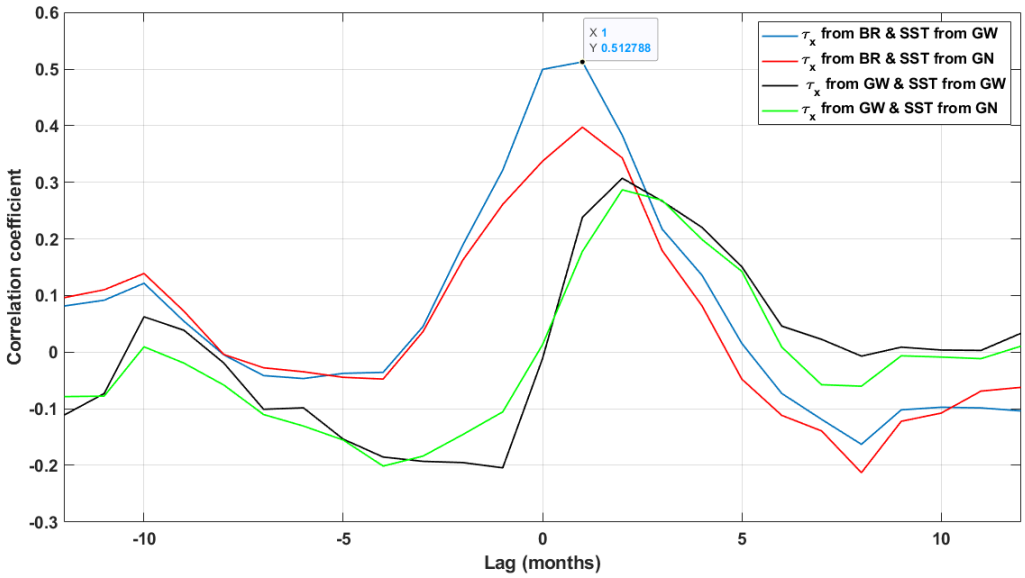

Figure 14: Lag correlation between τ_x and SST from satellite observations for the different regions (see legend).

The lag correlations from observations for the selected regions are displayed in Figure 14 and look similar to the lag correlation obtained by *Servain et al.* [1982], who used 60-year time series from 1911 to 1972. The fact that the highest correlation occurs between $\Delta\tau_x$ from the Brazilian region and SST from the Gulf of Guinea region (GW) suggests the plausibility that the SST signals during upwelling are influenced by a remote source around the Brazilian region. A similar lag correlation analysis using data from ECCO is shown in Figure 15, and looks very much like those obtained from the satellite observations. By comparing Figures 14 and 15, and the results of *Servain et al.* [1982], we see that increasing the duration of the time series provides a better representation of lag correlations.

8 Conclusions

In this research, we analyzed upwelling events from time series of about 20 to 36 years in the Gulf of Guinea using satellite altimeter data and ECCO model output. Our

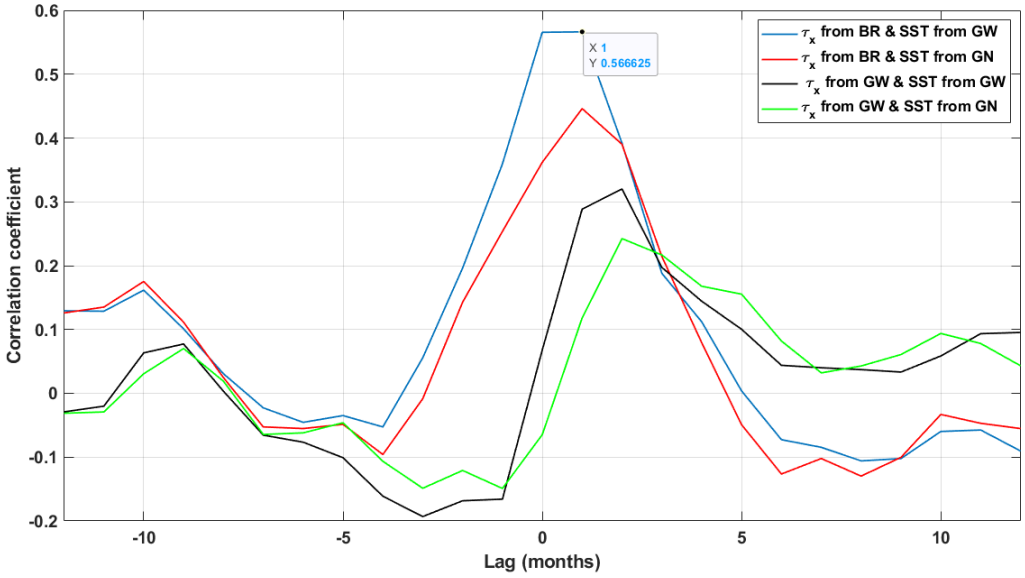

Figure 15: Lag correlation between τ_x and SST from ECCO for different regions (see legend).

analysis helps to zero in on the causes of upwelling in the Gulf of Guinea. Early historical discussions of the possible causes of upwelling events in the eastern Atlantic region and the Gulf of Guinea used limited observational data and simple numerical model outputs to analyze and study upwelling events (e.g., *Moore et al.* [1978], *O'Brien* [1978], *Servain et al.* [1982], *Picaut* [1983], and *Adamec et al.* [1978]). *Adamec et al.* [1978] had issues with the irregular geometry of the equatorial Atlantic basin, which approximately extends 5000 km zonally, and 1500 km on either side of the equator, leading to some errors in the numerical model. Such errors are minimized in the ECCO model, making the model more realistic than previous models.

Moore et al. [1978], *O'Brien* [1978], *Adamec et al.* [1978] and *Picaut* [1983] suggested that upwelling events in the Gulf of Guinea are not associated with local winds. This is because upwelling in the Gulf of Guinea is different from the classical (theoretical) case of wind and Ekman transport. They hypothesized that upwelling in the Gulf of Guinea results from Kelvin waves propagating eastward from the Brazillian coast along the equator. The equatorially trapped Kelvin waves reach the eastern coast of Africa and then propagate along the coastal boundary of West Africa as coastally trapped Kelvin waves.

This research uses SSH (SLA), SST, and wind data from the satellite (observations) and ECCO (model) data. One of the research questions was to determine how well Kelvin waves in the Gulf of Guinea region are predicted from the output of the ECCO model. We found that there were some years where the satellite observational results correlated well with model data for the extracted Kelvin waves. This research also helps to provide some documentation of the signatures of Kelvin waves in satellite observations and ECCO output in the Gulf of Guinea region.

Servain et al. [1982] discussed the relationship between the wind stress from the Brazilian region and SST anomalies from the Gulf of Guinea region. Their results indicated that the upwelling is due to events closer to the Brazilian coast. In this research, a similar analysis was done using relatively recent data from 1981 to 2016 to obtain a 36-year time series for the wind stress anomaly in the Brazilian region and the SST anomaly from the Guinea-west region. We also use output from a state-of-the-art global ocean model to study this phenomenon, in contrast to *Servain et al.* [1982] who used only satellite data. The lag correlation is similar to the lag correlation obtained in *Servain et al.* [1982] which used 60-year time series. ECCO data from 1993 to 2016 produced a 24-year time series. We find that the lag correlations from ECCO are also similar to those from observations, with the highest correlations occurring between the zonal wind stress from the Brazilian region and the SST signals from the Gulf of Guinea region. This provides some hope that ECCO could be used to make predictions of upwelling in the Gulf of Guinea.

Further work is still needed in the future to properly link the equatorial Kelvin waves that reach the eastern part of Equatorial Guinea and propagate west to the Gulf of Guinea to cause upwelling. Once the connection between the equatorial Kelvin waves and upwelling events in the Gulf of Guinea has been bridged, the results could be used to predict upwelling events on the West African coast. This will help measure, if possible, the strength of upwelling events over time and will help fully understand the causes of the minor and major upwelling seasons in the region.

Other studies suggests some contribution of local winds to the Gulf of Guinea upwelling. Another future endeavour would be to determine the fraction of upwelling caused by these local winds versus those attributed to remote forcing by Kelvin waves.

9 Acknowledgements

The authors are grateful to Dr Michael McPhaden for his insightful view of the upwelling dynamics in the equatorial Atlantic region during a summer school organized by ECCO on May 19-31, 2019, at Friday Harbor, Washington, USA. Special thanks to Prof. Paulo S. Polito for making available the code used in characterizing Rossby waves. We thank the various data sources for the freely available data (the SLA data was obtained from E.U. Copernicus Marine Service Information `https://doi.org/10.48670/moi-00145`, SSH and SST data were obtained from NASA Jet Propulsion Laboratory at `https://ecco.jpl.nasa.gov/drive/files/Version5/Alpha/latlon_daily/SSH.nc` and `https://ecco.jpl.nasa.gov/drive/files/Version5/Alpha/latlon_daily/SST.nc`, and the ERA5 wind product and SST were obtained from Copernicus Climate Change Service (C3S) Climate Data Store (CDS) at `https://cds.climate.copernicus.eu/cdsapp#!/dataset/reanalysis-era5-single-levels?tab=form`). We also acknowledge support from National Science Foundation grants OCE-1351837, OCE-1851164, and Office of Naval Research grant N00014-22-1-2570. This research was undertaken at the Department of Mathematics, University of Ghana, Legon, with support from the Building a New Generation of Academics in Africa (BANGA-Africa).

References

Abrahams, A., Schlegel, R.W., and Smit A.J. (2021): Variation and Change of Upwelling Dynamics Detected in the World's Eastern Boundary Upwelling Systems, *Front. Mar. Sci.*, 8:626411. `https://doi:10.3389/fmars.2021.626411`.

Adamec, D., and J.J. O'Brien, 1978: The seasonal upwelling in the Gulf of Guinea due to remote forcing, *J. Phys. Oceanogr.,* 8, 1050-1060.

Arnault, S., Menard, Y., and Merle, J. (1990): Observing the Tropical Atlantic Ocean in 1986–87 from altimetry, *Journal of Geophysical Research*, 95, 17,921–17,946.

Arnault, S. and Cheney, R. (1994): Tropical Atlantic sea level variability from GEOSAT (1985–1989), *Journal of Geophysical Research*, 99, 18,207–18,223.

Bakun, A., 1978: Guinea Current upwelling, *Nature*, 271, 147-150.

Benoit, C. R. and Beckers, J.M. (2011): Introduction to Geophysical Fluid Dyanmics, *Academic Press*.

Binet, D. (1997): Climate and pelagic fisheries in the Canary and Guinea Currents 1964–1993: The role of trade winds and the Southern Oscillation, *Oceanol. Acta*, 20, 177–190.

Binet, D. and Servain, J. (1993): Have the recent hydrological changes in the Northern Gulf of Guinea induced the Sardinella aurita outburst?, *Oceanologica Acta*, vol. 16, no. 3, pp. 247–260. Retrieve from `https://archimer.ifremer.fr/doc/00099/21052/18678.pdf`.

Bunker, A. F. (1976): Computations of surface energy flux and annual air-sea interaction cycles of the North Atlantic Ocean, *Mon. Wea. Rev.*, 104, 1122–1140.

Busalacchi, A. and Picaut, J. (1983): Seasonal variability from a model of the tropical Atlantic ocean, *Journal of Geophysical Research*, 13, 1564–1588.

CMEMS (2019): Global ocean gridded L4 sea surface heights and derived variables reprocessed (1993-ongoing), *Copernicus Marine Environment Monitoring Service*, `https://doi.org/10.48670/moi-00148`.

Colin, C. (1970): Coastal upwelling events in front of the Ivory Coast during the FOCAL program, *Oceanol. Acta*, 11, 125–138.

Djakouré, S., P. Penven, B. Bourlès, V. Koné , and J. Veitch, 2017: Respective Roles of the Guinea Current and Local Winds on the Coastal Upwelling in the Northern Gulf of Guinea, *American Meteorological Society,* 108(C1), 47, 1367 – 1387, doi: 10.1175/JPO-D-16-0126.1.

Ducet, N., LeTraon, P.–Y., and Reverdin, G. (2000): Global high resolution mapping of ocean circulation from TOPEX/Poseidon and ERS–1/2, *Journal of Geophysical Research*, vol. 105, no. C8, pp. 477–498.

Forget, G. A. E. L., Campin, J. M., Heimbach, P., Hill, C. N., Ponte, R. M., and Wunsch, C. (2015): ECCO version 4: An integrated framework for non-linear inverse modeling and global ocean state estimation. *Geoscientific Model Development*, 8(10), 3071-3104, `doi:10.5194/gmd-8-3071-2015`.

Franca .C., Wainer, I., Mesquita, A. R. and Goni, G. (2003): Planetary equatorial trapped waves in the Atlantic ocean from TOPEX/POSEIDON altimetry, *Elsevier Oceanography Series*, 68, 213–232,946. `https://doi.org/10.1016/S04229894(03)801484`.

Franca .C., I. Wainer, A. R. Mesquita, and G. Goni: Planetary equatorial trapped waves in the Atlantic ocean from TOPEX/POSEIDON altimetry.

Hersbach, H., Bell, B., Berrisford, P., Biavati, G., Horányi, A., Muñoz Sabater, J., Nicolas, J., Peubey, C., Radu, R., Rozum, I., Schepers, D., Simmons, A., Soci, C., Dee, D., and Thépaut, J–N. (2018): ERA5 hourly data on single levels from 1959 to present. Copernicus Climate Change Service (C3S) Climate Data Store (CDS), (Accessed on 22–Oct–2020), https://doi:10.24381/cds.adbb2d47.

Huang, B., Liu, C., Banzon, V. F. Freeman, E., Graham, G., Hankins, B., Smith, T. M., and Zhang, H.–M. (2020): NOAA 0.25–degree Daily Optimum Interpolation Sea Surface Temperature (OISST), Version 2.1. [https://www.ncei.noaa.gov/data/seasurfacetemperatureoptimuminterpolation/v2.1/access/avhrr/]. NOAA National Centers for Environmental Information. https://doi.org/10.25921/RE9PPT57. Accessed on 20th October 2021.

Houghton, R.W. (1976): Circulation and hydrographic structure over the Ghana continental shelf during the 1974 upwelling. Journal of Physical Oceanography, 6(6), 909–924.

Hurlburt, H.E. and Thompson, J.D. (1976): A numerical model of the Somali current, *Journal of Physical Oceanography*, 6, 646–664.

Ingham, M. (1970): *Coastal upwelling in the northwestern Gulf of Guinea*, *Bull. Mar. Sci.*, 20, 1–34.

Katz, E.J., Belevitsch, R., Bruce, J., Bubnov, V., Cochrane, J., Duing, W., Hisard, P., Lass, H.U., Meincke, J., DeMesquita, A., Miller, L., and Rybnikov, A. (1977): Zonal pressure gradient along the equatorial Atlantic, *J. Mar. Res.*, 35(2), 293–307.

Katz, E., and Garzoli, S. (1982): Response of the western equatorial Atlantic Ocean to an annual wind cycle, *J. Mar. Res.*, 40, 307–327.

Kindle, J.C. and O'Brien, J.J. (1976): A numerical simulation of the onset of E1 Nino, *Journal of Physical Oceanography*, 6, 621–631.

Knauss, J. A. (1997): Introduction to physical oceanography, *Waveland Press.*

Kouadio, Y.K., S. Djakouré, A. Aman, E. Ali, V. Kone, and E. Toualy, 2013: Characterization of the Boreal Summer Upwelling at the Northern Coast of the Gulf of Guinea Based on the PROPAO In Situ Measurements Network and Satellite Data, *International Journal of Oceanography.*

Lamb, P.J. (1978): Case studies of tropical Atlantic surface circulation pattern during recent sub– Saharan weather anomalies, 1967–1968, *Monthly Weather Review*,

vol. 106, pp. 482–491.

Lin, L. and Hurlburt, H. (1981): Maximum simplification of nonlinear Somali Current dynamics, *Monsoon dynamics*, pp.541–555.

Liu, W.T. (2002): Progress in scatterometer application, *Journal of Oceanography*, vol. 58, no. 1, pp. 121–136. https://doi.org/10.1023/A:1015832919110.

McCreary, J. (1976): Eastern tropical ocean response to changing wind systems; with application to El Nino, *Journal of Physical Oceanography*, 6(5), 632–645.

McPhaden, M. J. 2002: Mixed Layer Temperature Balance on Intraseasonal Timescales in the Equatorial Pacific Ocean. *Journal of Climate*, 15(18), 2632–2647. Retrieved Jul 23, 2022, from https://journals.ametsoc.org/view/journals/clim/15/18/15200442_2002_015_2632_mltboi_2.0.co_2.xml.

Moore, D. (1968): Planetary–gravity waves in an equatorial ocean, Ph.D. Thesis, Harvard University, Cambridge, Mass.

Moore, D.W. and Philander, S.G.H. (1977): Modeling of the tropical oceanic circulation, *The Sea, Vol. VI, John Wiley Interscience*, 319–361.

Moore, D.W., P. Hizard, J. McCreary, J. Merle, J.J. O'Brien, J. Picaut, J.M. Verstraete and C. Wunsch,, 1978: Equatorial adjustment in the eastern Atlantic, *Geophy. Res. Lett.,* 5, no. 8, pp. 637–640.

Nykjaer, L. and Van Camp, L. (1994): Seasonal and interannual variability of coastal upwelling along northwest Africa and Portugal from 1981 to 1991, *Journal of Geophysical Research*, vol. 99, no. C7, pp. 14197–14207.

O'Brien, J.J., D. Adamec, and D.W. Moore, 1978: A simple model of equatorial upwelling in the Gulf of Guinea, *Geophysical Research Letters*, 5, 641-644.

Oliveira S.C. and P.S. Polito, 2013: Characterization of westward propagating signals in the South Atlantic from altimeter and radiometer records, *Remote Sensing of Environment,* 134 (2013), 367 – 376.

Philander, S. G. H., 1979: Upwelling in the Gulf of Guinea, *J. Mar. Res.*,37:23–33.

Picaut, J., 1982: Propagation of the seasonal upwelling in the eastern equatorial Atlantic, *J. Phys. Oceanogr*, 18–37, https://doi.org/10.1175/1520-0485(1983)013<0018:POTSUI>2.0.CO;2.

Polito, P. S., and P. Cornillon, 1997: Long baroclinic Rossby waves detected by TOPEX/POSEIDON, *J. Geophys. Res.,* 102, 3215–3235, http://doi:10.1029/96JC03349.

Polito, P. S. and W. T. Liu, 2003: Global characterization of Rossby waves at several spectral bands, *J. Geophys. Res.*, 108(C1), 3018, http://doi:10.1029/2000JC000607.

Polito, P. S, O. T. Sato, and W. T. Liu, 2000: Characterization and validation of heat storage variability from Topex/Poseidon at four oceanographic sites, *J. Geophys. Res.*, 105(C7), 16,911–16,921.

Polo, I., A. Lazar, B. Rodriguez-Fonseca, and S. Arnault, 2008: Oceanic Kelvin waves and tropical Atlantic intraseasonal variability: 1. Kelvin wave characterization, *J. Geophys. Res.,* 113, C07009, doi:10.1029/2007JC004495.

Polito, P. S., and W. T. Liu, 2013: Global characterization of Rossby waves at several spectral bands, *J. Geophys. Res.,* 108(C1), 3018, doi:10.1029/2000JC000607, 2003.

Rayner, N. A., Parker, D. E., Horton, E.B., Folland, C. K., Alexander, L. V., Rowell, D. P., Kent, E. C., Kaplan, A. (2003): Global analyses of sea surface temperature, sea ice, and night marine air temperature since the late nineteenth century, *Journal of Geophysical Research*,Vol. 108, No. D14, 4407 https://doi:10.1029/2002JD002670.

Reynolds, R. W., Smith, T. M., Liu, C., Chelton, D. B., Casey, K. S., and Schlax, M. G. (2007): Daily High–resolution Blended Analyses for sea surface temperature, *J. Climate*, 20, 5473–5496. Reynolds, R.W. 2009. What's new in version 2. Available online at http://www.ncdc.noaa.gov/oa/climate/research/sst/papers/oisst_daily_v02r00_version2features.pdf.

Reynolds, R. W., Banzon, V. F., and NOAA CDR Program (2008): NOAA Optimum Interpolation 1/4 Degree Daily Sea Surface Temperature (OISST) Analysis, Version 2. NOAA National Climatic Data Center. https://doi:10.7289/V5SQ8XB5. Accessed on 20th January 2021.

Stewart, R. (2008): Introduction to Physical Oceanography, *Open Textbook Library.*

Roundy, P. E., and G. N. Kiladis, 2006: Observed relationships between oceanic Kelvin waves and atmospheric forcing, *J. Clim.,* 19, 5253– 5271.

Servain, J., J. Picaut, and J. Merle, 1982: Evidence of remote forcing in the equatorial Atlantic Ocean, *J. Phys. Oceanogr.,* 12, 457 – 463.

Talley, L. D., Pickard, G. L., Emery, W. J., and Swift, J. H. (2011): Descriptive Physical Oceanography: An Introduction, *Burlington: Elsevier Science.*

Thomson, R. E. and Emery, W. J. (2014): Chapter 5 – Time Series Analysis Methods (Data Analysis Methods in Physical Oceanography(Third Edition)),*Elsevier*, 425–591. https://doi.org/10.1016/B9780123877826.000053, retrieved Jul 27, 2022, from https://www.sciencedirect.com/science/article/pii/B9780123877826000053.

Tulich S.N, G.N. Kiladis, and A. Suzuki-Parker, 2009: Convectively coupled Kelvin and easterly waves in a regional climate simulation of the tropics, *Clim. Dyn.,* 36:185–203, urlhttp://doi10.1007s00382-009-0697-2.

Verstraete, J. M. (1970): The seasonal upwelling in the Gulf of Guinea, *Progress Oceanography*, vol. 29, no. 1, pp. 1–60.

Wiafe, G., Yaqub, H. B., Mensah, M. A., and Frid, C. L. J. (2008): Impact of climate change on long–term zooplankton biomass in the upwelling region of the Gulf of Guinea, *ICES Journal of Marine Science*, Volume 65, Issue 3, Pages 318–324

Wiafe, G. and Nyadjro, E.S. (2015): Satellite Observations of Upwelling in the Gulf of Guinea, *IEEE Geoscience and Remote Sensing Letters*, 12, 1066–1070. https://https://doi.org/10.1109/LGRS.2014.2379474.

Wyrtki, K. (1975): El Niño–The dynamic response of the equatorial Pacific ocean to atmospheric forcing, *Journal of Physical Oceanography*, 5, 572–584.

Yoshida, K. (1959): A theory of the Cromwell Current and of equatorial upwelling, *J. Oceanogra. Soc. Japan*, 15, 154–170.

Zhang H., Menemenlis, D., and Fenty, I. (2018): ECCO LLC270 ocean–ice state estimate, http://doi.org/1721.1/119821, also available at https://ecco.jpl.nasa.gov/drive/files/Version5/Alpha/doc/ECCO_LLC270.pdf.